JOURNAL OF AIRCRAFT
Vol. 48, No. 2, March–April 2011

Modeling of Dynamic Loading of Morphing-Wing Aircraft

B. Obradovic* and K. Subbarao†
University of Texas at Arlington, Arlington, Texas 76019

DOI: 10.2514/1.C000313

The simulation of dynamic loads and required power is essential for the design of any morphing-wing aircraft, since it ultimately determines the feasibility of a given morphing configuration. In this paper a methodology suitable for numerical calculation of the dynamic loads for a morphing wing aircraft is presented. The approach taken is one of extending rigid-body dynamics to include time-varying terms. The dynamic loads are derived from Lagrange's equations of a morphing aircraft, modeled as a system of rigid bodies connected by actuated rotational and translational joints. The overall flight dynamics are also treated using the extended rigid-body dynamics approach, introducing morphing forces and moments to model the correct dynamics for a morphing aircraft. Aerodynamic loads are computed using a vortex-lattice method. The overall model is applied to a gull-wing aircraft performing a set of morphing-induced maneuvers. The resulting loads are analyzed, and the strict power requirements of the gull-wing aircraft are explained.

Nomenclature

$\mathbf{F}$	=	net force acting on aircraft
$\mathbf{F_1}$	=	morphing force associated with center of mass acceleration
$\mathbf{F_2}$	=	morphing force associated with Coriolis force
$\mathbf{F_3}$	=	morphing force associated with transverse
$\mathbf{F_4}$	=	morphing force associated with centrifugal force
$[\mathbf{H_i}]$	=	Hessian matrix of i-th panel center with respect to morphing variables
$\mathbf{h}$	=	angular momentum of aircraft
$[\boldsymbol{J}]$	=	moment of inertia tensor
$\mathbf{M}_j$	=	morphing moment j ($j \in \{1, 4\}$)
m	=	mass of aircraft
$\hat{\mathbf{n}}_i$	=	normal vector of the i-th panel
P^j	=	generalized momentum associated with j-th actuator
Q_{CM}	=	generalized actuator moment associated with center of mass motion
$Q_{\text{CM-Rate}}$	=	generalized actuator moment associated with rate of center of mass motion
Q_{Panels}	=	generalized actuator moment associated with panel motion
$Q_{\text{Panels-Rate}}$	=	generalized actuator moment associated with rate of panel motion
$\mathbf{R_f}$	=	position of body frame origin with respect to inertial frame
$\mathbf{R_{cm}}$	=	position of aircraft center of mass with respect to inertial frame
$\mathbf{r}$	=	position of a mass element within the body frame
$\tilde{\boldsymbol{r}}$	=	skew-symmetric matrix representation of r
$\mathbf{r_{cm}}$	=	position of aircraft center of mass within body frame
$\boldsymbol{\tau}_{\mathbf{ext}}$	=	total external moment acting on aircraft
$[\tilde{\boldsymbol{\omega}}]$	=	skew-symmetric matrix representation of $\boldsymbol{\omega}$
$\boldsymbol{\omega}$	=	angular velocity of body frame w.r.t the inertial frame
$\mathbf{V_f}$	=	velocity of origin of aircraft body frame
$\mathbf{v}'$	=	velocity of a mass element in the body frame (body frame derivative of r)
$\mathbf{x}_i$	=	position of center of i-th aircraft panel in body frame
$\boldsymbol{\Delta r_{cm}}$	=	displacement of aircraft center of mass from body frame origin
ρ	=	mass density (of air, or aircraft, depending on context)

Presented at the AIAA Atmospheric Flight Mechanics Conference, Toronto, Ontario, Canada, 2–5 August 2010; received 16 February 2010; revision received 9 November 2010; accepted for publication 25 November 2010.

*Dept. of Mechanical and Aerospace Engineering; borna.obradovic@gmail.com. Student Member AIAA.

†Associate professor, Dept. of Mechanical and Aerospace Engineering; subbarao@uta.edu. Lifetime Member AIAA.

I. Introduction

A. Background

THE subject of morphing-wing aircraft has received considerable attention, and various morphing schemes have been proposed. The goals of morphing are either mission-optimization through change of wing shape, or rapid maneuvering made possible by large and rapid changes in the wing geometry. The key limiters to progress in the area are the potentially large power consumption and the actuator moments required to execute the morphing. It is therefore of great interest to be able to simulate the moments and power for a given morphing configuration and maneuver. Aircraft size, morphing rate, morphing geometry, and flight dynamics all play a role in determining the dynamic loads and power, making the subject quite complex and perhaps best suited for numerical simulation.

B. Technical Detail and Literature Survey

The conventional approach to studying a complex body such as a morphing-wing aircraft is one of the many flavors of multibody dynamics [1–6] (MBD). The aircraft is then modeled as an assemblage of rigid bodies constrained by revolving or sliding joints. Depending on the particular flavor of MBD chosen, the result is either a large and sparse differential-algebraic system (augmented MBD [1,5,6]), or contains a minimal set of differential equations, but entails a considerable effort in assembly at each time-step (embedded MBD [1–4]). Both approaches result in considerable computational effort. This effort is easily justified if the simulation goals include full structural dynamics. However, if the objective is to simulate (for example) a flight control system while taking into account the actuator loads and power, the MBD approaches are perhaps excessively CPU-intensive. The approach taken in this paper is to use extended rigid-body dynamics [7] for the system dynamics, and to derive analytic expressions for the dynamic loads of an arbitrary morphing-wing aircraft, starting from Lagrange's equations of motion. The actuator dynamics are partially specified (referred to as program constraints or servoconstraints) [8]. The "partial"

specification stems from the fact that external loads (aerodynamic and inertial) are not considered in the actuator dynamics. In effect, the morphing elements are assumed to have an internal control system, allowing them to behave as simple second-order dynamic systems [8], irrespective of the external loads. This leaves open the question of the actuator moments and power required to achieve the desired behavior. This has been investigated in the framework of MBD in a general context (not specific to morphing aircraft) [9,10]. While a number of studies have examined the flight dynamics of morphing aircraft [11–18], the subject of morphing-induced loads has received relatively little attention. In this work, the required actuator moments and power are studied using extended rigid-body dynamics, and analytic expressions that are functions of the aircraft and the morphing state are obtained. While the resulting expressions are analytic, they are not in algebraic closed form, and some terms require numerical integration over the volume of the aircraft. Additionally, the aerodynamic loads are obtained numerically using a quasi-unsteady vortex-lattice calculation [18–23] at each time step. As described in this paper and previously [7], the numerical integration incurs only a small CPU time penalty, while considerable savings are made through the reduced size of the ordinary differential equation system (as compared with MBD approaches). The most significant savings are obtained for complex aircraft.

II. Modeling of Flight Dynamics

The flight dynamics are modeled using extended rigid-body dynamics [7]. For completeness, the approach is summarized below.

The equations of motion of a time-varying body are derived, using a body frame attached to a fixed point on the aircraft (rather than at the center of mass, or CM). It is then shown that the standard Newton–Euler system is obtained, but with additional moments and forces. These are termed "morphing" moments and forces, and they depend on the motion of the CM within the aircraft body frame and the time-varying inertia tensor, as well as the details of the velocity and acceleration of mass elements within the body frame. Only the final results are shown here; the complete derivation is presented in earlier work [7]. The reference frames used and their relation to the CM is illustrated in Fig. 1.

1. *Rotational Equations of Motion*

The rotational equations of motion with morphing are shown to be:

$$[\mathbf{J}]\dot{\omega} = \boldsymbol{\tau}_{\mathbf{ext}} - [\tilde{\boldsymbol{\omega}}][\mathbf{J}]\boldsymbol{\omega} + \sum_{i=1}^{4} \mathbf{M_i} \tag{1}$$

The terms in the sum on the right-hand side (RHS) of Eq. (1) are the morphing moments, not present in the standard Euler Equations for rigid-body motion. Explicitly, they arise from the displacement of the CM from the body frame origin, the rate of change of the inertia tensor, and the body frame motion of mass within the aircraft.

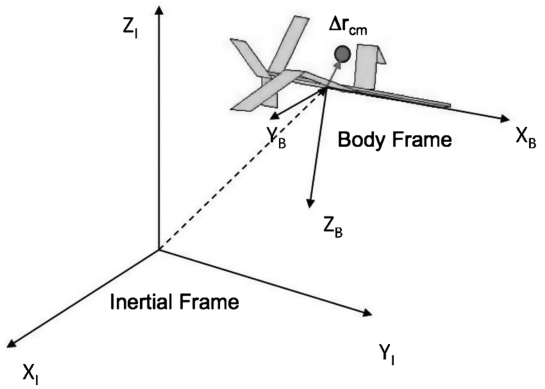

Fig. 1 Reference frames and instantaneous location of the CM are illustrated.

They are computed as follows:

$$\mathbf{M_1} = -[\dot{\mathbf{J}}]\boldsymbol{\omega} \tag{2}$$

$$\mathbf{M_2} = -m[\Delta\tilde{\boldsymbol{r}}_{\mathbf{cm}}]\cdot(\dot{\mathbf{V}}_{\mathbf{f}} + [\tilde{\boldsymbol{\omega}}]\mathbf{V_f}) \tag{3}$$

$$\mathbf{M_3} = -[\tilde{\boldsymbol{\omega}}]\int[\tilde{\mathbf{r}}]\mathbf{v}'\,\mathrm{d}m \tag{4}$$

$$\mathbf{M_4} = -\int[\tilde{\mathbf{r}}]\dot{\mathbf{v}}'\,\mathrm{d}m \tag{5}$$

For the special case of the rigid body, the morphing moments vanish, the inertia tensor is constant, and the rotational dynamics revert to the Euler equations. The final two terms involve nontrivial integrals and must be treated numerically. Only the M_4 term is actually significant (at least for the aircraft considered in this paper) [7].

2. *Translational Equations of Motion*

The translational dynamics are handled in much the same way as the rotational dynamics. Using the extended rigid-body dynamics approach, the Newton equation of motion for the CM of the aircraft is recast as an equation of motion for the body frame origin, with additional forces present to account for morphing. The equation of motion of the CM is simply given as:

$$\dot{\mathbf{V}}_{\mathbf{f}} = \frac{\mathbf{F_{ext}}}{m} + \mathbf{g} - [\tilde{\boldsymbol{\omega}}]\mathbf{V_f} + \frac{1}{m}\sum_{i=1}^{4}\mathbf{F_i} \tag{6}$$

The forces in the summation in Eq. (6) are the morphing forces, and are expressed as follows:

$$\mathbf{F_1} = -m\Delta\ddot{\mathbf{r}}_{\mathbf{cm}} \tag{7}$$

$$\mathbf{F_2} = -2m[\tilde{\boldsymbol{\omega}}]\Delta\dot{\mathbf{r}}_{\mathbf{cm}} \tag{8}$$

$$\mathbf{F_3} = -m[\dot{\tilde{\boldsymbol{\omega}}}]\Delta\mathbf{r}_{\mathbf{cm}} \tag{9}$$

$$\mathbf{F_4} = -m[\tilde{\boldsymbol{\omega}}][\tilde{\boldsymbol{\omega}}]\Delta\mathbf{r}_{\mathbf{cm}} \tag{10}$$

Only the F_1 and F_2 terms are significant, with F_2 dominating in the case of rapid morphing [7].

III. Modeling of Actuation and Dynamic Loads

In the scheme presented, actuator dynamics are modeled by a simple second-order system, the details of which are not subject to external loading. Physically, this corresponds to a controlled actuator, in which a model-following control system is used for each actuator. The control system then ensures that the actuator behaves according to the equations of the second-order system, in spite of the presence of aerodynamic, inertial, and morphing moments. The primary constraints are the required joint moments, peak power, and total energy consumption. Furthermore, knowledge of the actuator moments and power is useful in the design of an optimal aircraft control system, where it would be used to penalize actuator deflections. We thus seek the generalized force on each actuator, which is required to follow the second-order actuator dynamics. The result is necessarily approximate, but is suitable for comparisons of moments and required power for different morphing schemes, as well as for the design of control systems and optimal maneuver trajectories which need to take power into account.

To model the actuator, state variables for the actuator displacements $\{q_1, q_2, \ldots, q_n\}$ are introduced. Since the equations of translational dynamics involve the second derivative of the CM displacement (itself a function of the configuration variables), a second-order system is used to describe the dynamics of each configuration variable. Thus, we also define the state variables $\{p_1, p_2, \ldots, p_n\}$, with $p_i = \dot{q}_i$. The desired or control input set is then $\{q_{c1}, q_{c2}, \ldots, q_{cn}\}$. Thus the model for the actuator is chosen as

$$\dot{p}_i = -2\xi_i\omega_i p_i - \omega_i^2(q_i - q_{ci}) \tag{11}$$

$$\dot{q}_i = p_i \tag{12}$$

with the parameters ω and ξ suitably chosen to model the response of each actuator.

The governing equations of motion for the morphing aircraft are constructed using Lagrange's equations of motion. Each actuator variable (morphing coordinate) is assigned to a generalized coordinate q^j. The overall Lagrangian includes additional generalized coordinates, but it is the morphing coordinates that are of interest for actuator dynamics. Lagrange's equation for the jth actuator can then be written as:

$$\frac{\mathrm{d}P^j}{\mathrm{d}t} = \frac{\partial T}{\partial q} + Q^j + Q^j_{\text{ext}} \tag{13}$$

where Q^j is the generalized force associated with the jth generalized coordinate (one of the morphing state variables), and P^j is the associated generalized momentum. The generalized force Q^j_{ext} represents the aerodynamic portion of the load (aerodynamic and gravitational), and it is computed explicitly from the vortex-lattice aerodynamics solution. Since the dynamics of the problem are known (the required generalized forces are postprocessed after the dynamics at each time step), the term $\frac{\mathrm{d}P^j}{\mathrm{d}t}$ can be computed at run time from the state vector. Thus, Eq. (13) can be simply rearranged to yield an expression for the generalized actuator force in terms of known (computable) quantities:

$$Q^j = \frac{\mathrm{d}P^j}{\mathrm{d}t} - \frac{\partial T}{\partial q} - Q^j_{\text{ext}} \tag{14}$$

To use Eq. (14), expressions for $\frac{\mathrm{d}P^j}{\mathrm{d}t}$ and $\frac{\partial T}{\partial q^j}$ are required. Using the definition of generalized momentum, we have:

$$\frac{\mathrm{d}P^j}{\mathrm{d}t} = \frac{\mathrm{d}}{\mathrm{d}t}\left(\frac{\partial T}{\partial \dot{q}^j}\right) \tag{15}$$

The kinetic energy part of the Lagrangian is obtained as:

$$T = T_f + \frac{1}{2}\boldsymbol{\omega}^T[\boldsymbol{J}]\boldsymbol{\omega} + T_{\text{morph}}(q, \dot{q}) \tag{16}$$

where T_f is the kinetic energy of the translational velocity of the body frame, $\frac{1}{2}\omega^T J\omega$ is the rotational energy of the body frame, and T_{morph} is the kinetic energy of the intrabody-frame motion of the morphing aircraft components. Specifically, we have:

$$T = \int \frac{1}{2}\|\mathbf{V_f} + \mathbf{v}\|^2 \,\mathrm{d}m = \int \frac{1}{2}(\|\mathbf{V_f}\|^2 + \|\mathbf{v}\|^2 + 2\mathbf{V_f}\cdot\mathbf{v})\,\mathrm{d}m \tag{17}$$

$$T = T_f + \int\left(\frac{1}{2}\|\mathbf{v}\|^2 + \mathbf{V_f}\cdot\mathbf{v}\right)\mathrm{d}m \tag{18}$$

The term $\mathbf{v}$ in Eq. (18) represents the velocity of a mass element of the aircraft, including both the rotational velocity of the body frame and the intrabody-frame morphing velocity. The first term T_f is the kinetic energy due to the translational motion of the body frame, and it does not explicitly depend on any morphing state variables. Thus, it will not contribute directly to the generalized force. The second term in Eq. (18) is further expanded as follows:

$$\begin{aligned}\int \frac{1}{2}\|\mathbf{v}\|^2\,\mathrm{d}m &= \int \frac{1}{2}\|[\tilde{\boldsymbol{\omega}}]\boldsymbol{r} + \mathbf{v}'\|^2\,\mathrm{d}m \\ &= \int \frac{1}{2}[\|[\tilde{\boldsymbol{\omega}}]\boldsymbol{r}\|^2 + \|\mathbf{v}'\|^2 + 2[\tilde{\boldsymbol{\omega}}]\boldsymbol{r}\cdot\mathbf{v}']\,\mathrm{d}m \\ &= \frac{1}{2}\boldsymbol{\omega}^T[\mathbf{J}]\boldsymbol{\omega} + \frac{1}{2}\int\|\mathbf{v}'\|^2\,\mathrm{d}m + \int([\tilde{\boldsymbol{\omega}}]\boldsymbol{r})\cdot\mathbf{v}'\,\mathrm{d}m\end{aligned} \tag{19}$$

The third and final term of Eq. (18) can be further expressed as:

$$\begin{aligned}\mathbf{V_f}\cdot\int\mathbf{v}\,\mathrm{d}m &= \mathbf{V_f}\cdot\int([\tilde{\boldsymbol{\omega}}]\boldsymbol{r} + \mathbf{v}')\,\mathrm{d}m \\ &= \mathbf{V_f}\cdot\int([\tilde{\boldsymbol{\omega}}]\boldsymbol{r})\,\mathrm{d}m + \mathbf{V_f}\cdot\int\mathbf{v}'\,\mathrm{d}m \\ &= \mathbf{V_f}\cdot m[\tilde{\boldsymbol{\omega}}]\boldsymbol{\Delta r_{cm}} + m\mathbf{V_f}\cdot\boldsymbol{\Delta}\dot{\mathbf{r}}_{\mathbf{cm}}\end{aligned} \tag{20}$$

Thus, the complete kinetic energy of the morphing aircraft can then be summarized as:

$$\begin{aligned}T = T_f &+ \frac{1}{2}\omega^{\mathbf{T}}[\mathbf{J}]\omega + \frac{1}{2}\int\|\mathbf{v}'\|^2\,\mathrm{d}m + \int([\tilde{\boldsymbol{\omega}}]\boldsymbol{r})\mathbf{v}'\,\mathrm{d}m \\ &+ \mathbf{V_f}\cdot m[\tilde{\boldsymbol{\omega}}]\boldsymbol{\Delta r_{cm}} + m\mathbf{V_f}\cdot\boldsymbol{\Delta}\dot{\mathbf{r}}_{\mathbf{cm}}\end{aligned} \tag{21}$$

The first two terms in Eq. (21) are recognized as the translational and rotational kinetic energy arising due to body frame motion, and are present even for rigid aircraft. The remaining terms arise due to morphing. The generalized momentum associated with the jth state variable can then be expressed as:

$$P^j = \frac{\partial T}{\partial \dot{q}^j} = m\mathbf{V_f}\cdot\frac{\partial\boldsymbol{\Delta}\dot{\mathbf{r}}_{\mathbf{cm}}}{\partial\dot{q}^j} + \int([\tilde{\boldsymbol{\omega}}]\boldsymbol{r})\frac{\partial\mathbf{v}'}{\partial\dot{q}^j}\,\mathrm{d}m + \int\mathbf{v}'\frac{\partial\mathbf{v}'}{\partial\dot{q}^j}\,\mathrm{d}m \tag{22}$$

where only terms that are explicit functions of the morphing state variable derivatives are included. Noting that the term $\mathbf{v}'$ is the body frame temporal derivative of the position vector $\mathbf{r}$ and simplifying, we have:

$$P^j = m\mathbf{V_f}\cdot\frac{\partial\boldsymbol{\Delta}\dot{\mathbf{r}}_{\mathbf{cm}}}{\partial\dot{q}^j} + [\tilde{\boldsymbol{\omega}}]\int\mathbf{r}\frac{\partial\dot{\mathbf{r}}}{\partial\dot{q}^j}\,\mathrm{d}m + \int\mathbf{v}'\frac{\partial\dot{\mathbf{r}}}{\partial\dot{q}^j}\,\mathrm{d}m \tag{23}$$

The joints are assumed to enforce holonomic constrains only. Applying "cancellation of dots," we have:

$$P^j = m\mathbf{V_f}\cdot\frac{\partial\boldsymbol{\Delta r_{cm}}}{\partial q^j} + \int([\tilde{\boldsymbol{\omega}}]\boldsymbol{r} + \mathbf{v}')\frac{\partial\mathbf{r}}{\partial q^j}\,\mathrm{d}m \tag{24}$$

Finally, to obtain the generalized force in Eq. (13), the time derivative of Eq. (24) is performed. The obtained result is:

$$\begin{aligned}\dot{P}^j = &m(\dot{\mathbf{V}}_\mathbf{f} + [\tilde{\boldsymbol{\omega}}]\boldsymbol{V}_f)\cdot\frac{\partial\boldsymbol{\Delta r_{cm}}}{\partial q^j} + m\mathbf{V_f}\cdot\left(\frac{\partial\boldsymbol{\Delta}\dot{\mathbf{r}}_{\mathbf{cm}}}{\partial q^j} + [\tilde{\boldsymbol{\omega}}]\frac{\partial\boldsymbol{\Delta r_{cm}}}{\partial q^j}\right) \\ &+ \int([\tilde{\boldsymbol{\omega}}][\tilde{\boldsymbol{\omega}}]\boldsymbol{r} + 2[\tilde{\boldsymbol{\omega}}]\boldsymbol{v}' + [\dot{\tilde{\boldsymbol{\omega}}}]\boldsymbol{r} + \dot{\mathbf{v}}')\frac{\partial\mathbf{r}}{\partial q^j}\,\mathrm{d}m + \int([\tilde{\boldsymbol{\omega}}]\boldsymbol{r} \\ &+ \mathbf{v}')\left(\frac{\mathrm{d}}{\mathrm{d}t}\frac{\partial\mathbf{r}}{\partial q^j} + [\tilde{\boldsymbol{\omega}}]\frac{\partial\boldsymbol{\Delta r_{cm}}}{\partial q^j}\right)\mathrm{d}m\end{aligned} \tag{25}$$

From a computational standpoint with respect to geometrical derivatives, the various terms in Eq. (25) can be grouped into five categories: terms which depend on the geometrical derivatives of the CM, the time derivative of the geometrical derivatives of the CM, the geometrical derivatives of panel coordinates, the time derivative of the geometrical derivatives of panel coordinates, and finally, a mixed term which combines panel derivatives and CM derivatives. As will be demonstrated in Sec. IV, the terms involving time derivatives of the geometric derivatives (i.e., $\frac{\mathrm{d}}{\mathrm{d}t}\frac{\partial\Delta r_{\text{cm}}}{\partial q^j}$) are negligible (but are included for completeness).

To finalize the computation of the generalized force, the partial derivative of the kinetic energy [second term on RHS of Eq. (14)] is derived next:

$$\frac{\partial T}{\partial q^j} = \int \mathbf{v}' \frac{\partial \mathbf{v}'}{\partial q^j}\,\mathrm{d}m + \int [\tilde{\boldsymbol{\omega}}] \frac{\partial \mathbf{r}}{\partial q^j} \mathbf{v}'\,\mathrm{d}m + \int [\tilde{\boldsymbol{\omega}}] \boldsymbol{r} \frac{\partial \mathbf{v}'}{\partial q^j}\,\mathrm{d}m + m\mathbf{V}_\mathbf{f} \cdot [\tilde{\boldsymbol{\omega}}] \frac{\partial \boldsymbol{\Delta} \mathbf{r}_\mathbf{cm}}{\partial q^j} + m\mathbf{V}_\mathbf{f} \cdot \frac{\partial \boldsymbol{\Delta} \dot{\mathbf{r}}_\mathbf{cm}}{\partial q^j} \tag{26}$$

In Eq. (26), the first, third, and fifth terms on the RHS prove to be negligible (as shown in Sec. IV), since they represent mixed temporal and geometrical derivatives. The third term of Eq. (25) cancels the fourth term of Eq. (26). Likewise, the second term of Eq. (25) cancels the last term of Eq. (26). The second term of Eq. (26) is identical to the "Coriolis" term of Eq. (25) to within a prefactor, which, when added to Eq. (26), converts the Coriolis prefactor from two to three. Collecting the terms of Eqs. (25) and (26), and dropping the negligible and canceled terms, the various components of the generalized actuator force are summarized as:

$$Q_{\mathrm{CM}} = m \frac{\partial \boldsymbol{\Delta} \mathbf{r}_\mathbf{cm}}{\partial q^j} \cdot (\dot{\mathbf{V}}_\mathbf{f} + [\tilde{\boldsymbol{\omega}}] \mathbf{V}_\mathbf{f}) \tag{27}$$

$$Q_{\mathrm{Panel}} = \int ([\tilde{\boldsymbol{\omega}}][\tilde{\boldsymbol{\omega}}] \boldsymbol{r} + 3[\tilde{\boldsymbol{\omega}}] \boldsymbol{v}' + [\dot{\tilde{\boldsymbol{\omega}}}] \boldsymbol{r} + \dot{\mathbf{v}}') \frac{\partial \mathbf{r}}{\partial q^j}\,\mathrm{d}m \tag{28}$$

$$Q_{\mathrm{Panel\text{-}Rate}} = \int ([\tilde{\boldsymbol{\omega}}] \boldsymbol{r} + \mathbf{v}') \left(\frac{\mathrm{d}}{\mathrm{d}t} \frac{\partial \mathbf{r}}{\partial q^j} \right) \mathrm{d}m \tag{29}$$

$$Q_{\mathrm{Mixed}} = \int ([\tilde{\boldsymbol{\omega}}] \boldsymbol{r} + \mathbf{v}') [\tilde{\boldsymbol{\omega}}] \frac{\partial \boldsymbol{\Delta} \mathbf{r}_\mathbf{cm}}{\partial q^j}\,\mathrm{d}m \tag{30}$$

From a physical standpoint, Eqs. (27–30) contain two types of terms: those induced by morphing, and those that are purely inertial in nature. Terms which depend explicitly on morphing velocities or accelerations are present only in morphing aircraft. Inertial terms, which do not depend on the derivatives of morphing terms, exist in any aircraft type. Note that the term $m\dot{\mathbf{V}}_\mathbf{f} \frac{\partial \boldsymbol{\Delta} \mathbf{r}_\mathbf{cm}}{\partial q^j}$ is not a purely morphing term. The partial derivative of the CM with respect to joint angles is nonvanishing, even when the CM is never displaced from its original position. The geometrical derivative $\frac{\partial \boldsymbol{\Delta} \mathbf{r}_\mathbf{cm}}{\partial q^j}$ represents a sensitivity parameter which determines the degree of coupling of the CM motion to virtual displacements of the wing actuators. Thus, even for nonmorphing aircraft, this formalism is useful for studying the induced joint moments, as the first step in an flexibility analysis. The morphing and inertial contributions of the various Q-terms are summarized in Table 1.

Three types of derivatives appear in Eqs. (25) and (26): temporal derivatives of panel coordinates (or CM) such as $\dot{\mathbf{r}}_i$, purely geometrical derivatives such as $\frac{\partial \mathbf{r}_i}{\partial q^j}$, and time derivatives of the geometric derivatives, such as $\frac{\mathrm{d}}{\mathrm{d}t}(\frac{\partial \mathbf{r}_i}{\partial q^j})$. The first two derivative types are handled in a straightforward manner; the last is computed as follows:

$$\frac{\mathrm{d}}{\mathrm{d}t} \left(\frac{\partial \mathbf{X}}{\partial q^j} \right) = \sum_k \frac{\partial}{\partial q^k} \frac{\partial \mathbf{X}}{\partial q^j} \dot{q}^k = \sum_k = [\mathbf{H}]_{kj} \dot{q}^k \tag{31}$$

where the elements of the Hessian matrix $[\mathbf{H}]$ in Eq. (31) are the purely geometric second-order partial derivatives given by:

$$[\mathbf{H}]_{kj} = \frac{\partial^2 \mathbf{X}}{\partial q^k \partial q^j} \tag{32}$$

Table 1 Summary of actuator generalized force properties

Term Type	Q_{CM}	Q_{Panel}	$Q_{\mathrm{Panel\text{-}Rate}}$	Q_{Mixed}
Morphing	No	Yes	Yes	Yes
Inertial	Yes	Yes	No	Yes

and X is a placeholder for a panel coordinate, or the CM. Similarly, mixed temporal and geometrical derivatives appear in terms such as:

$$\frac{\partial \boldsymbol{\Delta} \dot{\mathbf{r}}_\mathbf{cm}}{\partial q^j} = \sum_k \frac{\partial^2 \boldsymbol{\Delta} \mathbf{r}_\mathbf{cm}}{\partial q^j \partial q^k} \dot{q}^k \tag{33}$$

which also require the computation of Hessian terms. It can be anticipated that terms which include the Hessian will be of lesser importance (this is verified by explicit simulation in Sec. IV). These expressions represent the second-order terms in the Taylor expansion of the functional dependence of panel coordinates (or the CM) on the morphing coordinates. Thus, we can write for a panel coordinate r_i:

$$\mathbf{r}_i(q_1, q_2, \ldots, q_n) = \mathbf{r}_i(q_{01}, q_{02}, \ldots, q_{0n}) + \nabla_q \mathbf{r}_i \cdot (dq_1, dq_2, \ldots, dq_n) + \sum_k \sum_j \frac{\partial^2 \mathbf{r}_i}{\partial q^j \partial q^k} dq^k dq^j + O(dq^3) \tag{34}$$

The second-order derivatives in Eq. (34) are negligibly small. Thus, neglecting these terms is equivalent to a first-order Taylor expansion of the transformation between body frame Cartesian coordinates and morphing coordinates. When the aircraft is operating close to a trim point, we can expect the second-order contributions to be small. Finally, the required power for each actuator can be computed simply as:

$$\frac{\mathrm{d}W_k}{\mathrm{d}t} = Q_k \dot{q}_k \tag{35}$$

IV. Application to Morphing-Wing Configurations

To test the utility of the simulation methodology, we apply it to several morphable-wing configurations. In each configuration, the conventional aileron and flap control surfaces have been replaced by movable wing sections. The basic properties of the simulated aircraft are summarized in Table 2. Two different conditions are examined. The first is a symmetric flattening of the wings, starting with the gull-wing configuration. This involves longitudinal dynamics only. The second case is a rapid turn maneuver, induced by asymmetric folding of the wings. In each case, the emphasis is on the induced dynamic loading on the wing actuators, as well as on the required power. A detailed study of the dynamics of the morphing maneuvers themselves has been presented previously [7].

The magnitudes of the CM Jacobian elements are illustrated in Table 3.

In this section, the dynamic loads are investigated for two flight maneuvers. The full morphing flight dynamics are used with vortex-lattice computed aerodynamic forces, and integrated over the simulated trajectory [7]. The complete set of aerodynamic and inertial loads are computed and discussed. One of the simulated maneuvers involves only symmetric morphing and longitudinal dynamics, whereas the other is an asymmetrically morphed turn maneuver.

Table 2 Gull-wing aircraft basic properties

Length	2 m
Wingspan	2 m
Area	0.87 cm^2
Mass	50 kg
I_{xx}	10 $\mathrm{kg\,m}^2$
I_{yy}	17 $\mathrm{kg\,m}^2$
I_{zz}	11 $\mathrm{kg\,m}^2$
I_{xz}	-1.8 $\mathrm{kg\,m}^2$
Mach Number (cruise)	0.2–0.25

Table 3 Actuator generalized coordinates to CM Jacobian

	L. Wing	L. Winglet	R. Wing	R. Winglet	L. Ruddervon	R. Ruddervon
CM_x	−0.0056	−0.0014	−0.0056	−0.0014	0.0034	−0.0034
CM_y	0.0202	−0.0101	−0.0202	0.0101	−0.0011	−0.0011
CM_z	−0.0709	−0.0177	−0.0709	−0.0177	0.0011	−0.0011

1. Symmetric Wing Flattening

The joint moments and power are investigated using nonlinear flight simulation. A simple symmetric flight condition involving only the longitudinal dynamics is examined first. The aircraft begins the maneuver with its wings in a symmetric gull-wing configuration, in trimmed, level flight. The wing configuration and aerodynamic forces are illustrated in Fig. 2.

At $t = 15$ s, the wings are rapidly lowered (symmetrically) to a nearly flat condition and then maintained in the lowered position for 5 s. The wings are then raised back into the symmetric gull-wing configuration. The wing and winglet deflections are shown in Fig. 3. The simulated trajectory and aircraft configuration are shown in Fig. 4. The fourth and fifth aircraft snapshots in Fig. 4 illustrate the lowered wing configuration. Note that the vertical scale is compressed, the relative change in altitude is quite small.

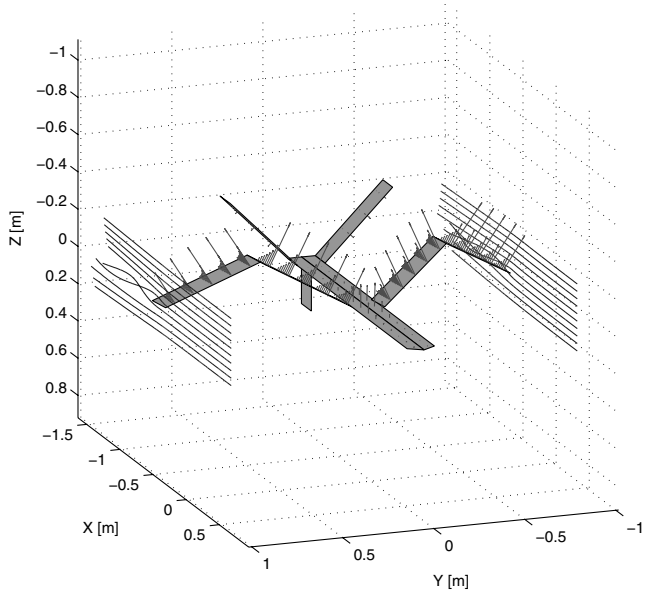

Fig. 2 The reference symmetric gull-wing configuration, with airflow streamlines and aerodynamic forces.

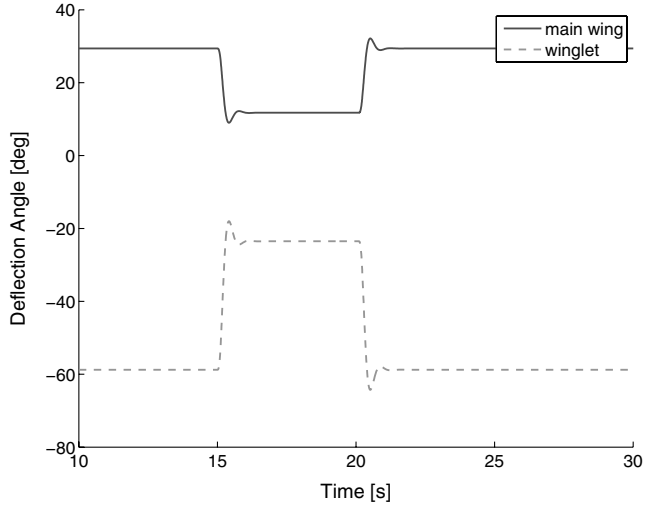

Fig. 3 Wing and winglet motion during the symmetric wing-flattening maneuver.

As expected, the increased lift with the flat wings results in the aircraft pitching upwards and gaining altitude, after which phugoidlike oscillation is observed. The detailed state of the aircraft during this maneuver is illustrated in Fig. 5. Because of symmetry, only longitudinal variables are involved in the dynamics. The pitch rate behaves largely as expected, with the exception of the negative pitch rate at the very beginning of the maneuver. This initial negative pitch rate is a result of the morphing moment M_4 (illustrated in Figs. 6 and 7).

As can be seen from Figs. 6 and 7, the expected aerodynamic pitch moment is slightly preceded by the morphing moment M_4, which acts in the opposite direction (for both the initial and final morphing). The morphing moment M_4 [Eq. (5)] is associated with the acceleration of mass elements within the body frame attached to the aircraft. As the wings are lowered, mass elements of the wings are accelerating downward. This implies a finite rate of change of angular momentum around the Y-axis, which cannot take place without an applied moment in the Y-direction. The morphing moment therefore suppresses this change of angular momentum (at least initially).

Since the M_4 moment is driven by acceleration of mass elements, while the aerodynamic moment is controlled by their displacement, the M_4 moment tends to precede the aerodynamic moment. The sign of M_4 depends on the details of the wing placement with respect to the CM of the aircraft. For the aircraft simulated here, most of the mass of the wings is behind the body frame origin (the CM of the aircraft before morphing), resulting in an initial negative morphing moment. An examination of the time dependence of the morphing moment in Fig. 7 reveals a discontinuity in the slope. This is a consequence of modeling the actuators as second-order systems, which are then driven by step inputs in this particular example. However, any kind of input is possible in principle. It is of interest to note that a similar effect was previously observed [24], although this was not explored in great detail. The authors concluded that the pitching moment was an artifact of the control system (which may be the case), but the configuration of the aircraft suggests that an implicitly modeled morphing moment may be responsible.

The overall behavior of the actuator moments for each joint during the entire 60 seconds of flight is illustrated in Fig. 8. The abbreviations in Fig. 8 stand for left and right wing-winglet and wing-fuselage joints. From Fig. 8, it is apparent that there are five distinct time epochs that determine the qualitative behavior of the actuator moments: premorphing (up to $t = 15$ s), first morphing (time period between $t = 15$ and 16 s), intermorphing ($t = 16$–20 s) during which the effects of the morphed configuration are manifested, second morphing ($t = 20$–21 s), and postmorphing ($t = 21$ s and later), during which time the wings are in their original configuration. From Fig. 8, it is apparent that the aerodynamic joint moments are increased as the wings flatten. This is to be expected, since the overall lift is increased. The aerodynamic loads are therefore increased in the intermorphing phase, and this is reflected in the actuator moments. The wing-fuselage joint moments are necessarily larger than the wing-winglet moments, since the wing-fuselage joints must carry the entire wing load. The aerodynamic loads depend on the instantaneous position of the wings, and the wing panel velocities. The latter are functions of the velocity of the aircraft body frame origin, the angular velocity, as well as the morphing velocities of the panels. The inertial loads can be grouped into two categories: those with a significant nonmorphing component, and those that are primarily morphing-induced. The only actuator moment in the former category is Q_{CM}, which is seen to be significant even in the postmorphing

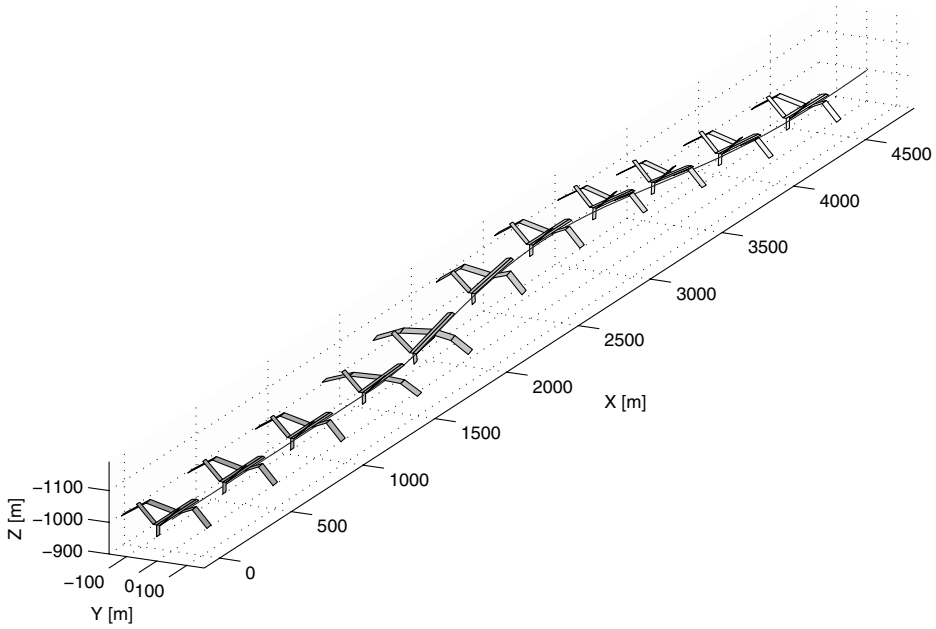

Fig. 4 Trajectory with symmetric wing flattening.

epoch. While some of the other moments do include purely inertial components (i.e., nonmorphing) as summarized in Table 1, their inertial contribution is quite small. Furthermore, the moment $Q_{\text{Panels-Rate}}$ is seen to be negligibly small, as anticipated in Sec. III. The Q_{CM} moment depends on the acceleration of the body frame origin (same for all actuators), modulated by a joint-dependent Jacobian term of the form $\frac{\partial \mathbf{r}_{\mathbf{cm}}}{\partial q_k}$. The Jacobian term measures how much the CM of the aircraft shifts due to a perturbation of the generalized morphing variable q_k (in the case of the gull-wing aircraft, all q_k variables are rotation angles). The magnitudes of Q_{CM} are therefore longitudinally symmetric, but the wing-fuselage joints require a larger moment (due to the larger overall impact on the CM). The overall behavior is modulated by the body frame origin acceleration, which is identical for all joints. The sign of the Q_{CM} moment can be understood as follows: at the onset of morphing, the aircraft accelerates upward, due to increased lift. Inertial forces therefore tend to push the wings downward [beyond the acceleration dictated by the morphing model of Eq. (11)]. The joint moment must therefore counter the inertial force and push the wings upward. In the sign convention used, upward rotation of the wings is considered positive. The positive joint moments persist during the inter-morphing period, as the aircraft continues to accelerate upward. The inertial term Q_{CM} therefore increases the overall load in this case (as evidence from Fig. 8). After the second morphing event, the aircraft begins to accelerate downward (due to reduced lift), and the sign of the Q_{CM} reverses for all joints. Q_{CM} then oscillates during the postmorphing phase as the aircraft executes the phugoidlike flight mode.

The morphing motion of the wing results in moments Q_{Panels} and Q_{Mixed} (the latter also includes a contribution from the morphing-induced CM motion). In both terms, the dominant contribution arises due to the body frame acceleration of the wing panels. As the wings

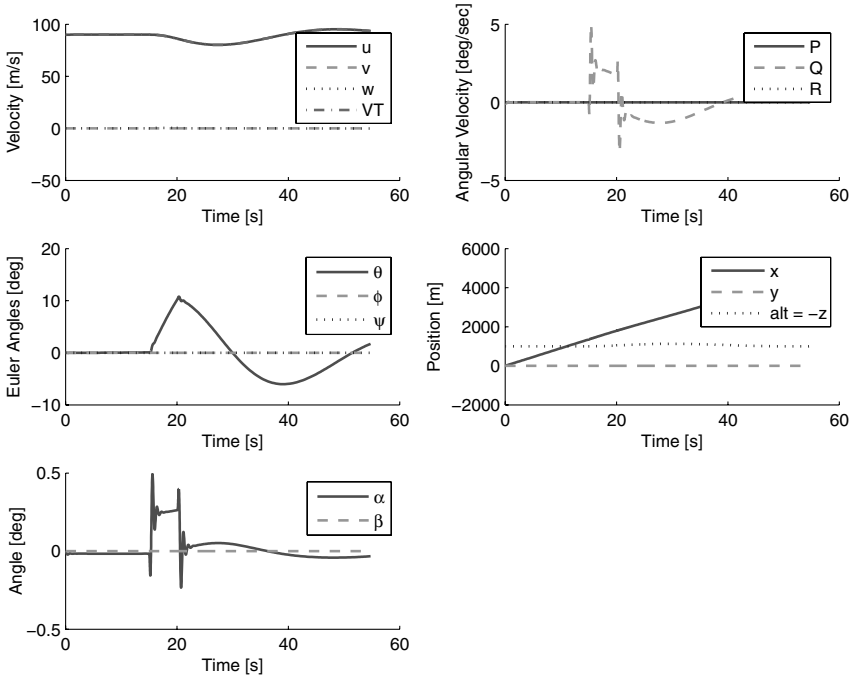

Fig. 5 Aircraft state during symmetric wing-flattening maneuver.

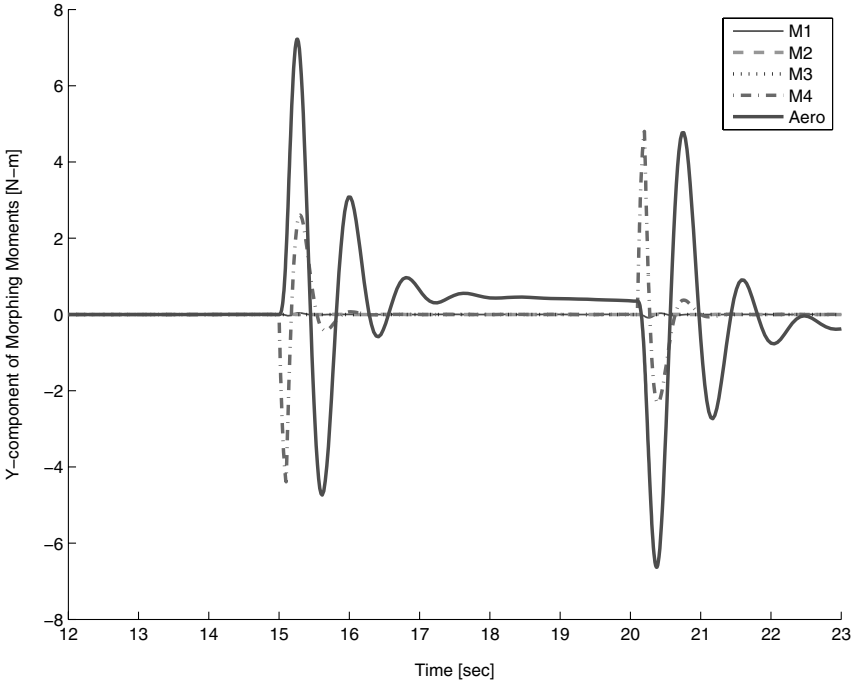

Fig. 6 Pitching moments acting on aircraft during initial morphing.

initially accelerate downward, the actuators must provide a negative moment (using the sign convention that positive angles increase the wing angle). As the wings slow down and settle into the flattened position, the required actuator moment becomes positive. The magnitudes of the morphing terms are comparable to the inertial Q_{CM} term in magnitude, but are of much shorter duration. The morphing terms are nonzero only during the morphing, whereas inertial terms are present whenever the body frame origin undergoes acceleration (and aerodynamic terms are present at all times).

The brief time period during which morphing takes place is particularly significant from the standpoint of power requirements. As is evident from Eq. (35), actuator power is required only during morphing. However, all generalized forces contribute during this time, not just the morphing terms (the Q_k of Eq. (35) is the total generalized force). The power required for the symmetric maneuver is illustrated in Fig. 9. The sign of the required power in Fig. 9 is at times negative, indicating work is done on the actuators. This is simply a consequence of the fact that, for a certain fraction of the time, the sum of aerodynamic and inertial forces is aligned with the desired acceleration of the wing panels (and the actuators consequently do negative work). However, this does not imply that the actuators are necessarily able to store this energy, unless a regenerative system is used. Thus, in general, energy will be expended during all phases of morphing motion, but the actual behavior during the negative power periods depends on the details of the actuators.

The magnitude of the required power depends on the morphing rate with (in principle) a stronger than linear dependence. At a minimum, Eq. (35) contains a linear dependence of the morphing rate

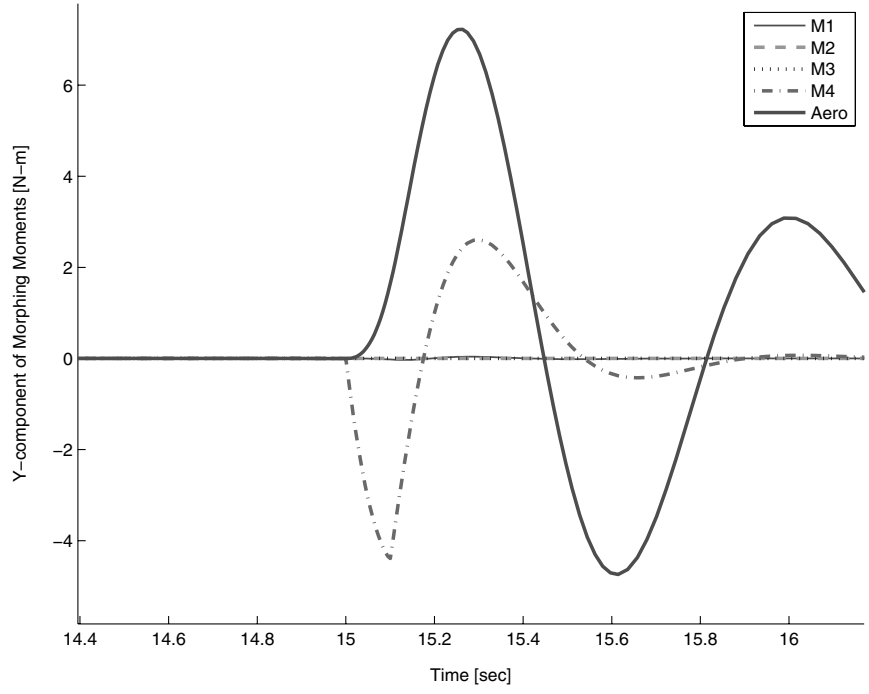

Fig. 7 Detailed view of pitching moments acting on aircraft during initial morphing.

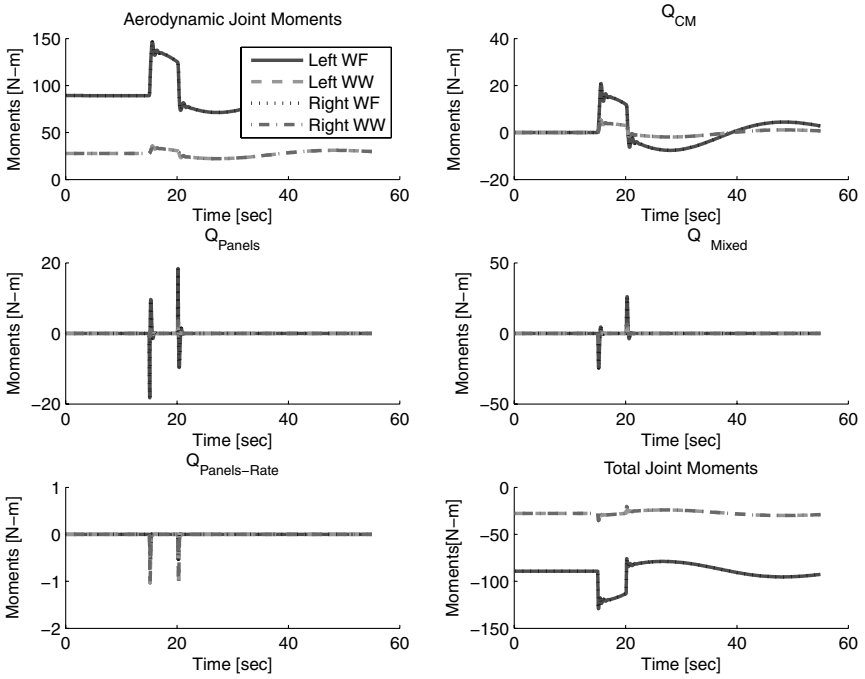

Fig. 8 Actuator moments for each joint during entire trajectory.

(through the $\dot{q}_k$ term). The generalized force Q_k of Eq. (35), however, is itself dependent on the morphing rate through the various morphing velocity and acceleration terms. Thus, we can expect the required power to be significantly decreased if the morphing rate is decreased. This is illustrated in Fig. 10, where the actuator bandwidth was reduced by a factor of 2 s. The peak required power is noticeably decreased. The dependence of the peak power requirement as a function of the actuator bandwidth is illustrated in Fig. 11.

In spite of the expected stronger than linear dependence of peak power on actuator bandwidth, Fig. 11 indicates that the dependence is very nearly linear. The reason is that the actuator moments are dominated by the aerodynamic component, which is not a function of the actuator bandwidth (to first order). This is a characteristic of morphing configurations in which the morphing motion is aligned with aerodynamic lift, as in the case of the gull-wing aircraft. Longitudinal morphing would result in less peak power and a stronger dependence on actuator properties. The behavior of the actuator moments and power during a rapid turn maneuver is examined next.

2. *Asymmetric Turn Maneuver*

The aircraft begins the maneuver in trimmed, level flight, with symmetrically folded gull wings, as illustrated in Fig. 2. At $t = 15$ s, only the left wing is lowered, as shown in Fig. 12. The time dependence of the wing angles is shown in Fig.13. The lift imbalance between the left and right wings produces a roll moment that results in a rapid turn, as illustrated in Fig. 14.

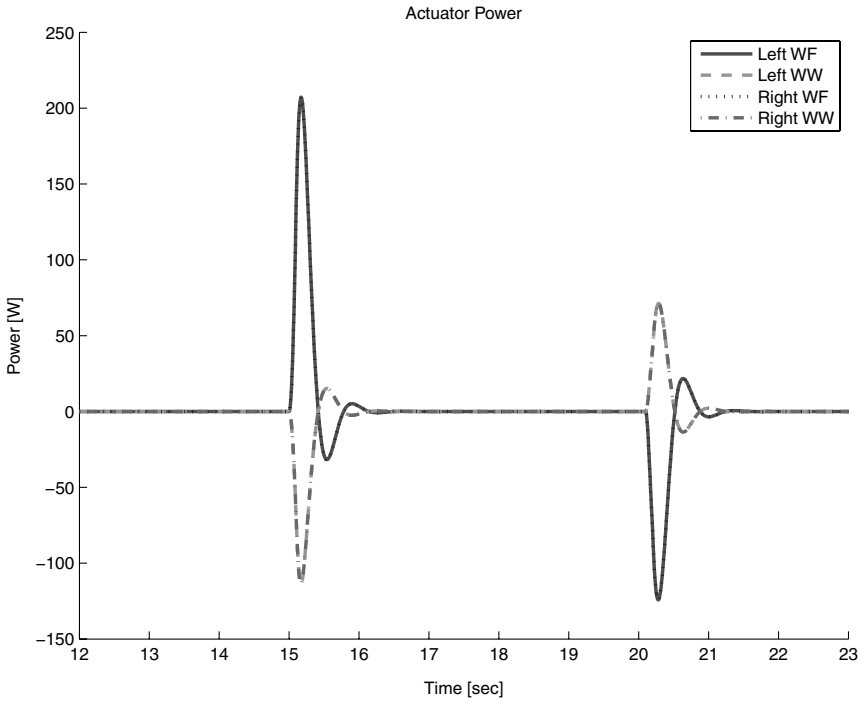

Fig. 9 Actuator power for each joint during morphing portion of the trajectory.

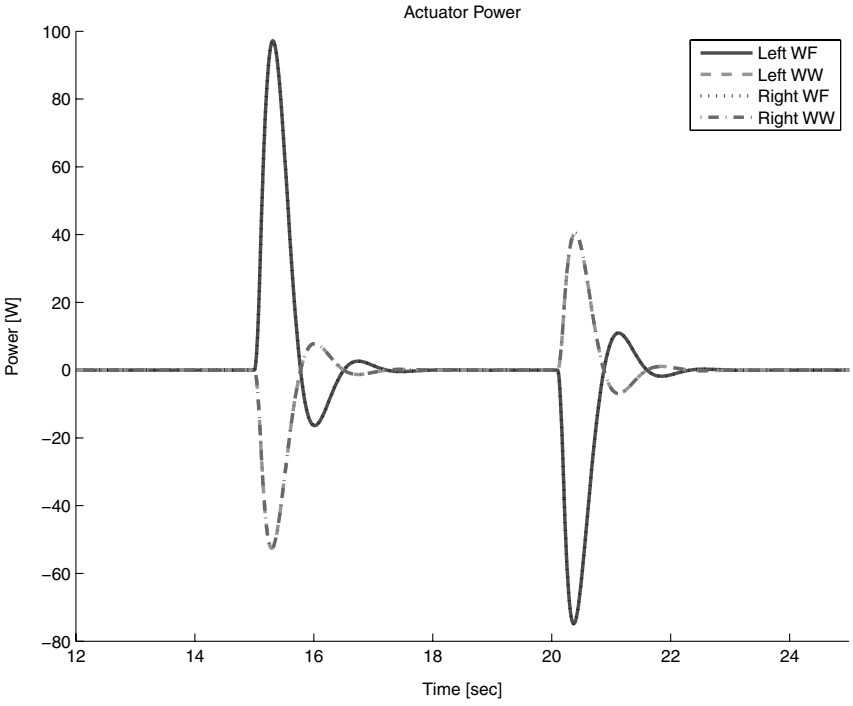

Fig. 10 Actuator power with slow morphing.

The overall behavior of the aircraft during the turn is illustrated in Figs. 14 and 15. The angular velocity exhibits the expected spike in roll, induced largely by aerodynamic moments. Morphing moments (particularly M_4) also play a significant role in the dynamics [7].

Much like the symmetric morphing case of Sec. IV.A.1, the behavior of the joint moments for the turn trajectory is best analyzed in three separate time epochs: the first 15 s before morphing, the 1.5 s of morphing, and the postmorphing remainder of the flight. Figure16 illustrates all three epochs, while Fig. 17 provides a closer view of the morphing epoch. From Fig. 16, it is evident that during the first 15 s (trimmed, level flight), aerodynamic forces are the only source of joint moments. The joint moments are symmetric, and the Wing-Fuselage moments are $\approx 4x$ larger than the wing-winglet moments (the aerodynamic loads and moment arm are each $\approx 2x$ at the wing root).

During the morphing epoch, the aerodynamic moments change dramatically. As the left wing flattens, the lift on it increases, resulting in a sharp rise in the left wing root moment (and to a somewhat lesser extent in the left wing-winglet moment). During this period, morphing-induced moments appear as well. While all terms from Eq. (25) contribute, the most significant are the terms involving the panel body frame accelerations (Q_{Panels}) and the acceleration of the body frame origin (Q_{CM}). The various joint moments are illustrated in Figs. 16 and 17. The moment required to flatten the left wing is evident in Fig. 17 (most evident in Q_{Panels}). A negative moment is required to initiate the flattening, followed by a positive moment to stop it. At the end of the morphing state, the opposite sequence takes place, with a positive moment initiating the return to the symmetric gull-wing configuration and a negative moment ending it (also most clearly seen in Fig. 17, Q_{Panels}). The dominant term in Eq. (25) driving this effect is the panel acceleration term. Also, we see in Fig. 17 the influence of inertial moments Q_{CM} on the

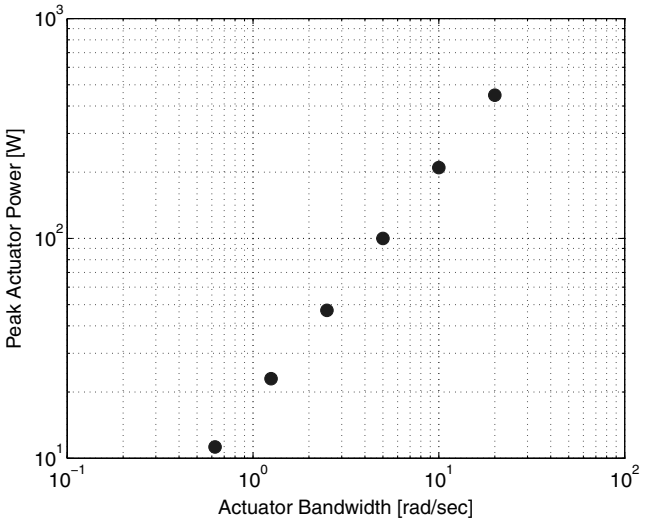

Fig. 11 Peak actuator power as a function of actuator bandwidth.

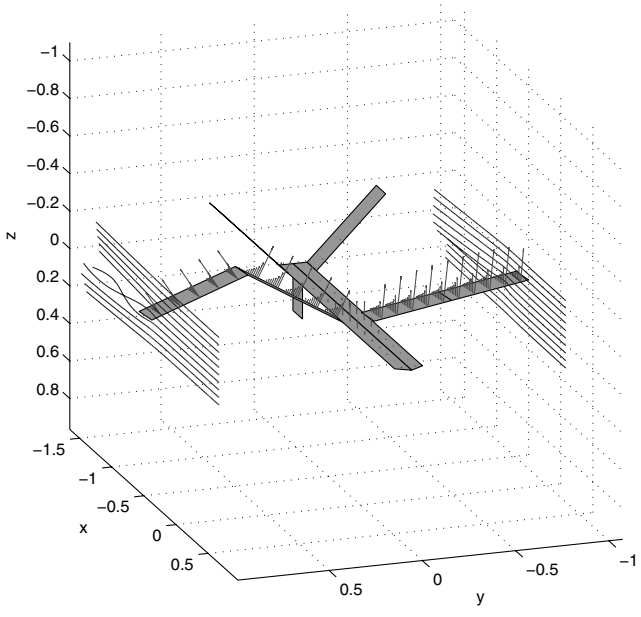

Fig. 12 The asymmetric gull-wing configuration, with airflow streamlines and aerodynamic forces.

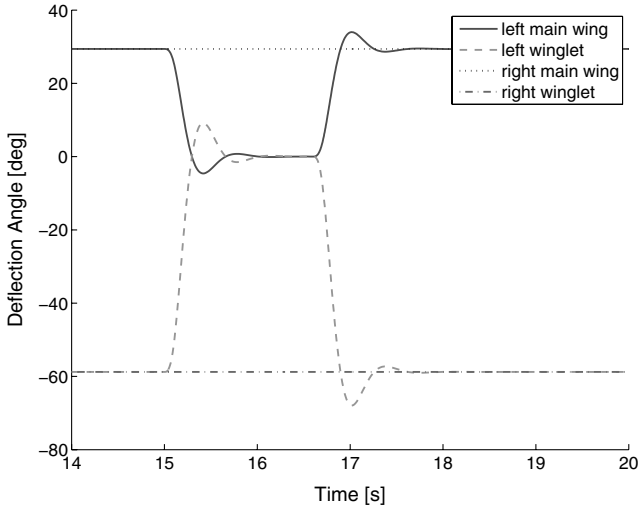

Fig. 13 Wing motion during the asymmetric turn.

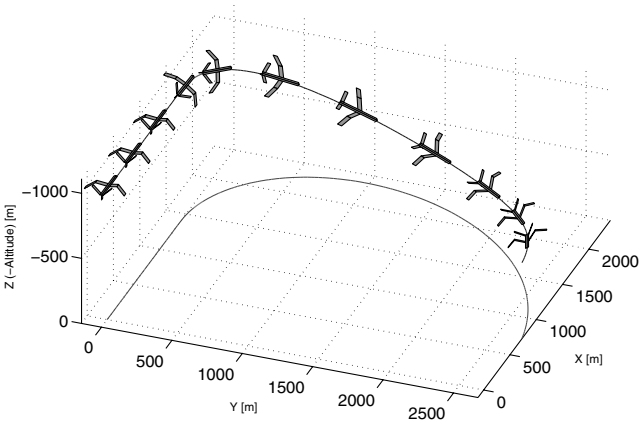

Fig. 14 The turning trajectory induced by asymmetric wing morphing.

right wing as well, in spite of the fact that it is not morphing. Particularly significant are the transverse acceleration (as the roll initiates) and the Y-direction motion of the CM (induced by the flattening of the left wing). Note that the effect is actually stronger on the right wing (which remains folded) than on the left wing (which flattens). This is caused by the larger coupling of the folded wing into the lateral motion of the CM. By the time the Q_{CM} moment peaks, the left wing is fully flattened. The acceleration vector during the turn is nearly parallel to the left wing, but the Jacobian for the left wing motion is nearly perpendicular to the wing (since the wing is almost flat at that point). Thus, the inner product of the Jacobian term and the acceleration vector which appears in the expression for Q_{CM} [Eq. (27)] is small. Finally, as the morphing epoch ends and the wings are returned to the symmetric gull-wing configuration, the influence of the inertial moments becomes more significant (as shown in Fig. 17 by Q_{CM}) than at the onset of morphing. This is simply due to the increased velocity and, particularly, the acceleration of the aircraft at this point in the trajectory (Fig. 15). As seen in the figure, both V_f and $\dot{V}_f$ are increased, due to the postmorphing dive and rapid turn.

After the completion of morphing, only aerodynamic and inertial forces contribute to the joint moments. As can be seen in Fig. 16, the aerodynamic moments increase (become more positive, turning the wings upward). The actuator moments preventing the wing motion are negative for both wings as the aircraft velocity increases, as evidenced by the plot of Fig. 16. The actuator moments during this epoch can be understood intuitively. The aircraft is still executing a turn (even though morphing has ceased), and the aerodynamic moments are pushing the wings toward the center of the turn (requiring a negative actuator moment to prevent that motion). At the same time, the inertial acceleration of the body frame Q_{CM} is bending the wings downward (requiring a positive actuator moment). Thus, the required actuator moment during the nonmorphing part of the turn is a balance between aerodynamic and inertial terms. The aerodynamic moment is dominant, but the net moment is significantly reduced during the turn, relative to what would have been predicted by aerodynamic loading alone.

The inertial moments on the various joints Q_{CM} are evidently quite different during the postmorphing epoch, in spite of the fact that the acceleration of the body frame is a common term for all of them. This is shown in Fig. 16. Mathematically, the difference is caused by the coupling coefficients to the CM motion, or more specifically, how it projects onto the acceleration of the body frame origin. Physically, the behavior is clearly understood from the aircraft state during the turn. The bank angle remains large for most of the turn, while the wings are folded in the symmetric gull-wing configuration. This means the right wing and the left winglet are essentially parallel to the body frame acceleration vector. Conversely, the left wing and right winglet are almost perpendicular to the acceleration vector (this is an exaggeration for the purpose of illustration; the actual difference in angles is not so pronounced). As a consequence, the moments

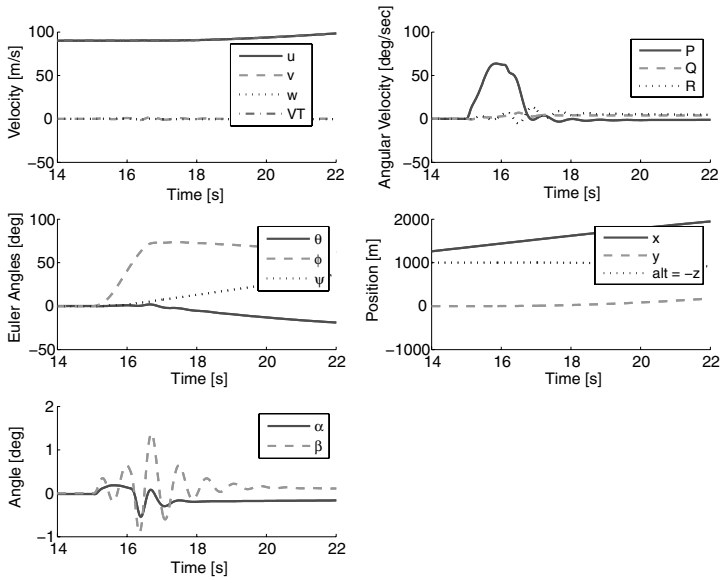

Fig. 15 The full state of the the aircraft during the morphing portion of the trajectory.

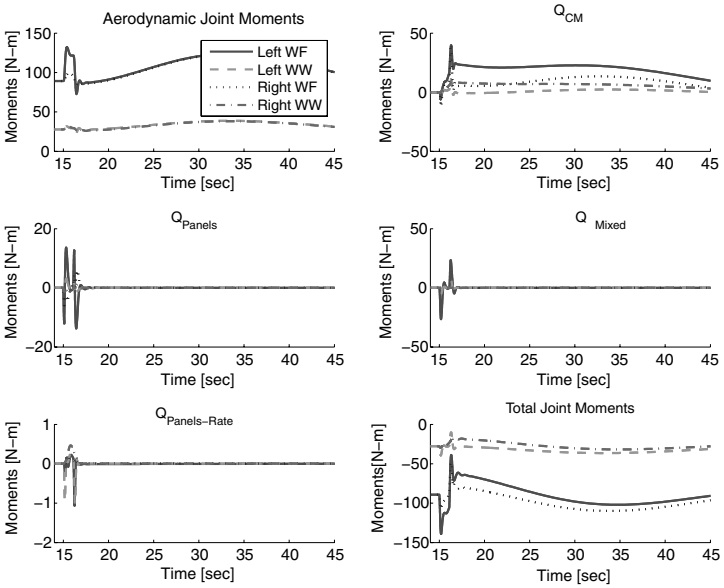

Fig. 16 Joint moments during the first 45 seconds of the trajectory.

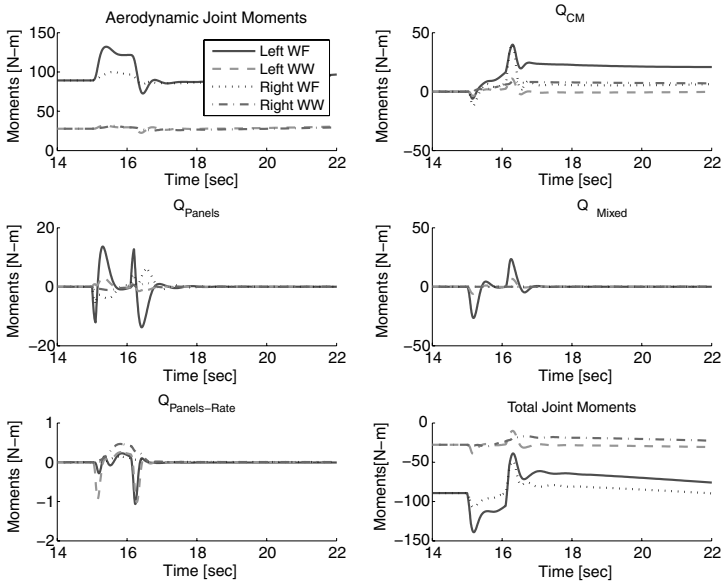

Fig. 17 Joint moments during the morphing phase.

required by the left winglet and right wing joint are reduced, relative to those of the left wing and right winglet.

V. Conclusions

A simulation methodology for computing the dynamic loading of morphing-wing aircraft has been developed. Aerodynamic, inertial, and morphing-induced loading effects were included, and can be applied to a wide variety of morphing configurations. The key quantities that must be computed are the Jacobian terms relating the coordinates of the various aircraft panels (as well as the CM) to the morphing variables. The morphing variables can represent actual (i.e., deliberate) morphing, or can simply represent virtual deformations of the aircraft. In the latter case, the computed actuator loads are in reality structural loads. Two morphing maneuvers were studied: a longitudinal heave and pitch maneuver, and a rapid turn maneuver. All maneuvers were open loop. The morphing-induced actuator loads were found to be significant, comparable in magnitude to the inertial terms. Aerodynamic loads, however, dominated the actuator loading during both types of maneuver. The power requirements for the maneuvers were also examined and found to be quite significant for rapid maneuvering with the gull-wing configuration. Much of the power requirement comes from the large impact of the aerodynamic moments, due to the lift-aligned morphing of the wings. It is suggested that longitudinal morphing would be preferable from a power standpoint.

References

[1] Shabana, A. A., *Dynamics of Multibody Systems*, 3rd ed., Cambridge Univ. Press, New York, 2005.

[2] Wittenburg, J., *Dynamics of Multibody Systems*, 2nd ed., Springer–Verlag, New York, 2002.

[3] Kane, T. R., and Levinson, D. A., *DYNAMICS: Theory and Applications*, 1st ed., McGraw–Hill, New York, 1985.

[4] Moon, F. C., *Applied Dynamics*, 1st ed., Wiley, New York, 2008.

[5] Fox, B., Jennings, L. S., and Zomaya, A., *Constrained Dynamics Computations: Models and Case Studies*, World Scientific Series in Robotics and Intelligent Systems, Vol. 16, World Scientific Publishing Co., Singapore, 2000.

[6] Blundell, M., and Harty, D., *Multi-Body Systems Approach to Vehicle Dynamics*, Butterworths, London, 2004.

[7] Obradovic, B., and Subbarao, K., "Modeling and Simulation to Study Flight Dynamics of a Morphable Wing Aircraft," AIAA 2009-6240, Aug. 2009.

[8] Seigler, T. M., and Neal, D. A., "Modeling and Flight Control of Large-Scale Morphing Aircraft," *Journal of Aircraft*, Vol. 44, No. 4, July–Aug. 2007, pp. 1077–1087.
doi:10.2514/1.21439

[9] Huston, R. L., Liu, C. Q., and Li, F., "Equivalent Control of Constrained Multibody Systems," *Multibody System Dynamics*, Vol. 10, No. 3, 2003.

[10] Blajer, W., "Dynamics and Control of Mechanical Systems in Partly Specified Motion," *Journal of the Franklin Institute*, Vol. 334B, No. 3, 1997, pp. 407–426.
doi:10.1016/S0016-0032(96)00091-9

[11] Weisshaar, T., "Morphing Aircraft Technology: New Shapes for Aircraft Design," Unclassified NATO Rept. RTO-MP-AVT-141, 2006.

[12] Davidson, J., Chwalowski, P., and Lazos, B., "Flight Dynamic Simulation Assessment of a Morphable Hyper-Elliptic Cambered Span Winged Configuration," AIAA 2003-5301, Aug. 2003.

[13] Valasek, J., Lampton, A., and Marwaha, M., "Morphing Unmanned Air Vehicle Intelligent Shape and Flight Control," AIAA 2009-1827, April 2009.

[14] Bowman, J., Sanders, B., and Weisshaar, T., "Evaluating the Impact of Morphing Technologies on Aircraft Performance," AIAA 2002-1631, April 2002.

[15] Grant, D., and Lind, R., "Effects of Time-Varying Inertias on Flight Dynamics of an Asymmetric Variable-Sweep Morphing Aircraft," AIAA 2007-6487, Aug. 2007.

[16] Grant, D., Abdulrahim, M., and Lind, R., "Flight Dynamics of a Morphing Aircraft Utilizing Independent Multiple-Joint Wing Sweep," AIAA 2006-6505, Aug. 2006.

[17] Chakravarthy, A., Grant, D., and Lind, R., "Time-Varying Dynamics of a Micro Air Vehicle with Variable-Sweep Morphing," AIAA 2009-6304, Aug. 2009.

[18] Yue, T., and Wang, L., "Multibody Dynamic Modeling and Simulation of a Tailless Folding Wing Morphing Aircraft," AIAA 2009-6155, Aug. 2009.

[19] Katz, J., and Plotkin, A., *Low-Speed Aerodynamics*, 2nd ed., Cambridge Univ. Press, New York, 2001.

[20] Bertin, J., and Smith, M., *Aerodynamics for Engineers*, Prentice-Hall, Inc., Englewood Cliffs, NJ, 1979.

[21] Wright, J., and Cooper, J., *Introduction to Aircraft Aeroelasticity and Loads*, John Wiley and Sons, New York, 2007.

[22] Melin, T., "Tornado, a Vortex Lattice MATLAB Implementation for Linear Aerodynamic Wing Applications," Master's Thesis, Royal Inst. of Technology (KTH), Sweden, 2000.

[23] Sequeira, C. J., Willis, D., and Peraire, J., "Comparing Aerodynamic Models for Numerical Simulation of Dynamics and Control of Aircraft," *AIAA Aerospace Sciences Meeting*, Reno, Nevada, 2006.

[24] Scarlet, J. N., Canfield, R. A., and Sanders, B., "Multibody Dynamic Aeroelastic Simulation of a Folding Wing Aircraft," AIAA 2006-2135, May 2006.